

● *Original Contribution*

## ASSESSMENT OF ARTERIAL STENOSIS IN A FLOW MODEL WITH POWER DOPPLER ANGIOGRAPHY: ACCURACY AND OBSERVATIONS ON BLOOD ECHOGENICITY

GUY CLOUTIER,<sup>\*†</sup> ZHAO QIN,<sup>\*</sup> DAMIEN GARCIA,<sup>\*</sup> GILLES SOULEZ,<sup>‡</sup> VINCENT OLIVA<sup>‡</sup>  
and LOUIS-GILLES DURAND<sup>\*</sup>

<sup>\*</sup>Laboratory of Biomedical Engineering, Institut de recherches cliniques de Montréal, University of Montréal, Montréal, Québec, Canada; <sup>†</sup>Laboratory of Biorheology and Medical Ultrasonics, Research Center and <sup>‡</sup>Department of Radiology, Centre Hospitalier de l'Université de Montréal, Montréal, Québec, Canada

(Received 20 March 2000; in final form 20 July 2000)

**Abstract**—The objective of the project was to study the influence of various hemodynamic and rheologic factors on the accuracy of 3-D power Doppler angiography (PDA) for quantifying the percentage of area reduction of a stenotic artery along its longitudinal axis. The study was performed with a 3-D power Doppler ultrasound (US) imaging system and an *in vitro* mock flow model containing a simulated artery with a stenosis of 80% area reduction. Measurements were performed under steady and pulsatile flow conditions by circulating, at different flow rates, four types of fluid (porcine whole blood, porcine whole blood with a US contrast agent, porcine blood cell suspension and porcine blood cell suspension with a US contrast agent). A total of 120 measurements were performed. Computational simulations of the fluid dynamics in the vicinity of the axisymmetrical stenosis were performed with finite-element modeling (FEM) to locate and identify the PDA signal loss due to the wall filter of the US instrument. The performance of three segmentation algorithms used to delineate the vessel lumen on the PDA images was assessed and compared. It is shown that the type of fluid flowing in the phantom affects the echoicity of PDA images and the accuracy of the segmentation algorithms. The type of flow (steady or pulsatile) and the flow rate can also influence the PDA image accuracy, whereas the use of US contrast agent has no significant effect. For the conditions that would correspond to a US scan of a common femoral artery (whole blood flowing at a mean pulsatile flow rate of 450 mL min<sup>-1</sup>), the errors in the percentages of area reduction were 4.3 ± 1.2% before the stenosis, -2.0 ± 1.0% in the stenosis, 11.5 ± 3.1% in the recirculation zone, and 2.8 ± 1.7% after the stenosis, respectively. Based on the simulated blood flow patterns obtained with FEM, the lower accuracy in the recirculation zone can be attributed to the effect of the wall filter that removes low flow velocities. In conclusion, the small errors reported *in vitro* may support the clinical use of this technique. © 2001 World Federation for Ultrasound in Medicine & Biology.

**Key Words:** Peripheral arterial disease, Lower limb arteries, Arterial stenosis, Power Doppler ultrasound, Blood echoogenicity, Computational fluid dynamics, 3-D reconstruction.

### INTRODUCTION

Duplex ultrasound (US) scanning has been the most widely applied noninvasive technique to quantify the severity of arterial stenoses. Several strategies were proposed to specifically evaluate lower limb arterial obstructions with this method (Allard et al. 1999; Aly et al. 1998b; Evans et al. 1989; London et al. 1999). The diagnosis with duplex scanning has been based on velocity waveform analysis, measurement of absolute ve-

locity, the characterization of Doppler spectral broadening, the detection of blood flow disturbances with color flow velocity imaging, and Doppler velocity ratio measurement. Although the use of modern US technologies may avoid the need for arteriography in some patients, recent studies showed limitations of duplex US for quantifying lower limb arterial lesions. For example, although controversial (Allard et al. 1999; Aly et al. 1998a; Sessler et al. 1996), the accuracy of duplex US may be limited in the case of multisegmental arterial lesions. Also, the quantification of the severity of stenoses in very distal segments (below the knee) and runoff vessels is difficult to assess with precision with US (Koelemay et al. 1997; Larch et al. 1997). Duplex or color Doppler US

Address correspondence to: Dr. G. Cloutier, Laboratoire de Génie Biomédical, Institut de Recherches Cliniques de Montréal, 110 Avenue des Pins Ouest, Montréal, Québec H2W 1R7 Canada. E-mail: cloutig@ircm.qc.ca and durandlg@ircm.qc.ca

measures the hemodynamic repercussions of arterial stricture (*i.e.*, acceleration at the site of the stenosis or dampening of the systolic upstroke downstream of the stenosis). Up to now, this information is not sufficient to plan surgical or endovascular therapy. Therefore, in most cases, digital subtraction or magnetic resonance angiography is required (Larch et al. 1997). Another alternative is power Doppler imaging, which gives a better demonstration of the vessel lumen than duplex US by estimating the integrated Doppler power spectrum (Rubin et al. 1994).

To our knowledge, power Doppler angiography (PDA) has never been clinically applied to quantify lower limb arterial stenoses. Three-dimensional PDA images of stenotic vessels were, however, obtained *in vitro* in steady and pulsatile flow models filled with a blood-mimicking fluid (Guo and Fenster 1996). The validation of the technique was extended by using porcine whole blood (Allard et al. 1997). In this last study, the degree and length of the stenosis obtained from the 3-D reconstruction of PDA images varied with the flow rate. In contradiction to what was observed with a blood-mimicking fluid (Guo and Fenster 1996), porcine blood echogenicity variations within PDA images seemed to affect the segmentation accuracy of the arterial lumen (Allard et al. 1997). Thus, the aim of this work was to study the influence of various hemodynamic and rheologic factors on the accuracy of 3-D PDA for arterial stenosis quantification, and to evaluate the effect of changes in blood echogenicity on the segmentation performance. Although PDA is introduced as a method to improve the assessment of lower limb arterial obstruction, the stenosis model is general and can be extended to other arterial segments.

## METHODS

### *Flow model and blood preparation*

The experiments were performed at room temperature in a horizontal mock flow model. A phantom containing a wall-less vessel surrounded by a tissue mimic made of water (89%), agar (3%) and glycerol (8%) was made to simulate a stenotic artery with an 80% area reduction. This phantom had an acoustic velocity similar to that of biologic tissue (Rickey et al. 1995). The diameter of the nonobstructed lumen was 7.96 mm. Pouring the molten tissue mimic around a rod, that was removed after the tissue mimic set, formed the wall-less vessel. The lumen diameter was measured with a micrometer on the rod used to create the lumen. The phantom does not absorb water and was preserved from drying; the lumen, thus, maintained its original dimension over time. The symmetrical stenosis had a cosine shape with a length of 20 mm. The inlet length of the wall-less vessel was

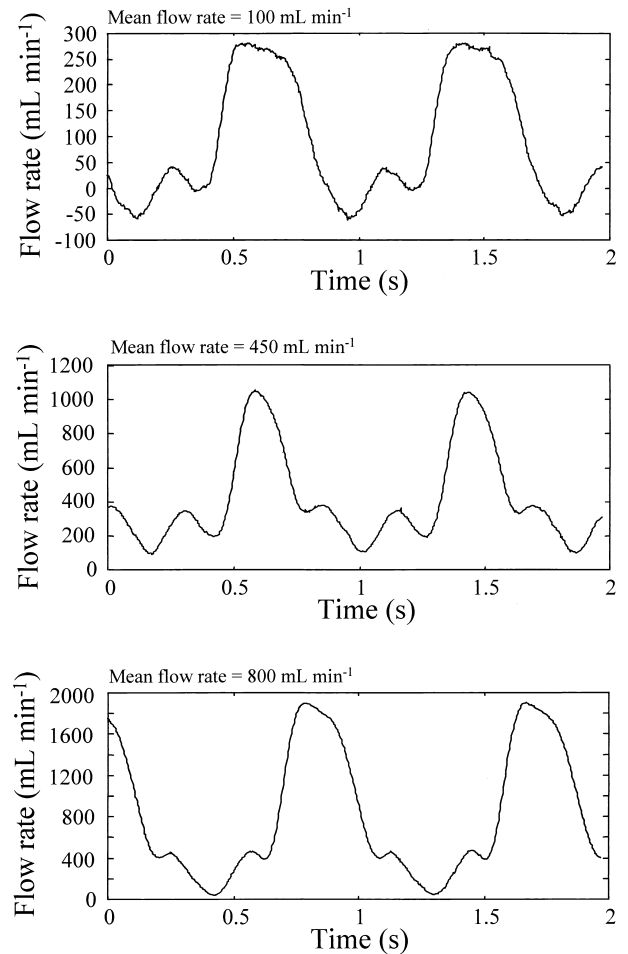


Fig. 1. Flow waveforms obtained for pulsatile flow experiments.

straight and long enough to ensure a fully developed laminar flow before the stenosis. Blood was circulated in the flow model with a roller pump for steady flow, and a pulsatile blood pump (Harvard Apparatus, South Natick, MA; Model 1421) for pulsatile flow. As described in Allard and Cloutier (1999), a damping reservoir located between the roller pump and the test section was used to eliminate oscillations for steady flow experiments. The flow rate was measured with a cannulating probe (Model SF625) coupled to an electromagnetic flowmeter (Cliniflow II, Model FM701D, Carolina Medical Electronics, King, NC). The stroke rate of the pulsatile pump was 70 beats/min and the phase ratio (% systole:% diastole) was 30:70. Examples of pulsatile flow profiles obtained at 100, 450 and 800 mL min<sup>-1</sup> are shown in Fig. 1.

Fresh porcine blood, collected from an abattoir, was anticoagulated with ethylenediamine-tetraacetic acid salt, the erythrocytes and buffy layers were separated by centrifugation, and the hematocrit was adjusted to 40%

by remixing the erythrocytes with plasma or a saline solution. Four types of fluid were circulated in the flow model (porcine whole blood, porcine whole blood with a US contrast agent, porcine blood cell suspension and porcine blood cell suspension with a US contrast agent). The blood suspension was prepared by washing and centrifuging blood cells twice with a 0.9% normal physiologic saline solution. The plasma was discarded, and the blood cells were resuspended in the saline solution before measurement. To reproduce the clinical situation of using an ultrasonographic contrast agent in suboptimal examinations, an ultrasound contrast agent (DMP-115, DuPont-Merck Pharmaceutical Co., N. Billerica, MA) was used in some experiments to enhance the backscattered power. The DMP-115 is a perfluoropropane gas-filled, lipid-encapsulated microbubble fluid that is stable in blood for several min. Before adding DMP-115 to blood, it was shaken for 45 s at room temperature to generate the bubbles. The concentration of DMP-115 used in all measurements was 0.03 mL/L of blood.

Experiments were conducted and repeated, with five different blood samples, for each flow condition (steady or pulsatile), and for each fluid used (whole blood or blood cell suspension). For each experiment, measurements were done with and without the US contrast agent at flow rates of 100, 450, and 800 mL min<sup>-1</sup>. Reported values of the flow rate at rest in the common femoral artery by using electromagnetic flowmeters are in the range of 100 to 660 mL min<sup>-1</sup> (Väntinen 1975). Much higher values were reported during exercise or papaverine injection (Dedichen and Kordt 1974; Hlavová *et al.* 1965). Thus, the experimental protocol allowed the simulation of femoral flow rates and the acquisition of a total of 120 3-D PDA volumes for statistical analysis.

#### *PDA image acquisition and preprocessing*

An ATL Ultramark 9 HDI US system with a 38-mm aperture linear-array probe (L7-4) was used for all cross-sectional PDA measurements. This probe was operated at 5 MHz for B-mode imaging and at 4 MHz in the Doppler power mode. The B-mode was used to identify the lumen of the vessel and to help in adjusting the intensity in PDA mode. Before each measurement, by adjusting the US-transmitted power and color gain, the flow field area of the PDA image proximal to the stenosis was matched visually to the lumen area observed in B-mode. Then, the tissue signal of the B-mode image was shut off to display only the flow field. In PDA mode, a pulse-repetition frequency (PRF) of 700 Hz was used to increase the imaging sensitivity. The lowest wall filter cut-off frequency (25 Hz) was selected because there was little wall movement in the phantom under pulsatile flow. The depth and zoom of the system were fixed for all experiments. The color sensitivity was maximum

(16), the dynamic image filtering option was not activated, the focal point was set near the center of the tube, the highest color priority was chosen, the persistence level was set to maximum (7) and the frame rate for these settings was 6 Hz. Because a linear grey-scale power map was used in PDA mode, the background noise was displayed as almost black and the flow field as grey levels related to the backscattered intensity.

A 3-D imaging system developed at the John P. Roberts Research Institute and produced by Life Imaging System Inc. (London, ON, Canada) was used for 3-D image acquisition and display. A discrete movement (0.5 mm) step motor was used to scan the wall-less artery longitudinally over a distance of 9.6 cm at a slow velocity of 0.25 mm/s. This slow scanning velocity ensured that each acquired image had no residual information from previous images due to the persistence level and low frame rate of the US instrument. A set of 192 cross-sectional 2-D PDA images was acquired at a Doppler angle of 70°. These 2-D images had a dimension of 256 × 256 pixels and were digitized with a precision of 8 bits/pixel. After acquisition, the PDA images were reconstructed perpendicular to the vessel axis following Doppler angle compensation. A total of approximately 180 slices was kept for 3-D visualization and analysis. The voxel dimensions were scaled by positioning two cursors in the x and y directions on the zoomed ATL screen, and by measuring their respective distance in mm and pixel number. The averaged voxel dimension of the 3-D volume was 0.095 × 0.085 × 0.5 mm<sup>3</sup> /pixel. No flow gating was performed by the instrument under pulsatile conditions.

#### *Segmentation algorithms*

In previous studies (Allard *et al.* 1997; Guo *et al.* 1998; Guo and Fenster 1996), thresholding based on the maximum intensity of each PDA image was used to segment the vessel lumen from the image background. Various threshold levels were tested between 10% to 75% of the maximum grey-level intensity of the PDA images. For the experimental conditions tested, a threshold of 25% of the maximum intensity was found to be a good selection to estimate the percentage of area reduction of the stenosis (Allard *et al.* 1997; Guo *et al.* 1998). To improve the characterization of the stenosis, two new segmentation algorithms were developed and their threshold adjusted to obtain the best performance in terms of percentage of area reduction. No optimization was performed on the absolute area because this parameter can be affected by the adjustment of the Doppler gain and transmitted power. Both the gain and transmitted power were kept constant for a given 3-D scanning. The description of each algorithm is given below:

1. This is the algorithm used in our previous studies. For each 2-D PDA image of the 3-D volume, the segmentation threshold was fixed to 25% of the maximum image intensity,  $I_{\max}$ . The flow area of each 2-D slice was calculated by counting pixels with intensities higher than the segmentation level. To compute the percentage of area reduction, a “normal nonobstructed cross-section” had to be determined and used as a reference area. For this purpose, the reference area was obtained by averaging the 10 largest area values of the whole 3-D volume. The percentage of area reduction,  $\%A_R$ , at a given location was computed by the following equation:

$$\%A_R = 100 \times \frac{A_{\text{ref}} - A}{A_{\text{ref}}}, \quad (1)$$

where  $A_{\text{ref}}$  is the reference area of the nonobstructed lumen computed from 10 PDA images, and  $A$  is the area of a given slice of the 3-D volume.

2. This segmentation method is an adaptive version of the first algorithm. It starts by using a segmentation level at 25% of  $I_{\max}$  for the reference area  $A_{\text{ref}}$ . Starting from the first slice, the segmentation level was then increased (or decreased) by steps of 5% each time the flow area of a given slice was reduced (or increased) by 10% compared to  $A_{\text{ref}}$ . This algorithm allows a segmentation level higher than 25% within the stenosis, which results in the removal of more pixels to compensate for the blurring of the PDA image due to the limited sample volume resolution of the instrument. For each slice, the percentage of area reduction was computed by using eqn (1).
3. A third algorithm was tested to take into consideration the distribution of the histogram image intensities of each PDA. The segmentation level was set to  $I_{\max}/0.3 I_{\text{mean}}$ , where  $I_{\text{mean}}$  is the mean image intensity of the histogram. The constant of 0.3 was the mean value that optimized the quantification of the percentage of area reduction, eqn (1), over all experimental conditions tested.

For all three algorithms, the segmentation level, in term of absolute image intensity, depends on  $I_{\max}$  and, thus, varies along the vessel segment.

#### Accuracy of the segmentation algorithms

To quantify the accuracy of each algorithm, the estimation errors on the area reduction were computed. The error was determined by:  $E_{AR} = \%A_R - \%A_{R(\text{true})}$ , where  $\%A_R$  is the percentage of area reduction given by eqn (1), and  $\%A_{R(\text{true})}$  is the true percentage of area reduction of the lumen (known from the dimensions of the flow phantom). The statistics (mean  $\pm$  standard de-

viation) for  $E_{AR}$  were computed over all experiments for four specific positions along the arterial lumen: 1. 4 cm before the central position of the stenosis ( $P_s$ ); 2. at  $P_s$ ; 3. 1 cm after  $P_s$ ; and 4. 5 cm after  $P_s$ . For positions 1, 3 and 4, the mean errors were obtained by averaging  $E_{AR}$  over 16 consecutive PDA images (image 1 corresponds to the position given above and image 16 to the downstream position shifted by 0.8 cm). For position 2, only the PDA image located at the central position of the stenosis was used for averaging purposes.

#### Modeling of the flow velocities and binary PDA images

At least two instrumental factors may limit the performance of the PDA method to delineate the vessel lumen. These factors are the limited resolution of the US system and the effect of the wall filter. A simulation model was developed to determine the signal loss on the PDA images due to the effect of the wall filter.

Finite-element modeling (FEM) of the flow velocities in the vicinity of the stenosis was performed with Fidap (Fluent Inc., Lebanon, NH, version 8). The entrance length, dimension, and shape of the stenosis simulated by FEM had the same characteristics as those of the *in vitro* model. The problem was 2-D axisymmetric and nonlinear, and the flow was considered laminar. The mesh of the flow region was composed of 6000 nodes and 5681 four-node quadrilateral elements. The successive substitution method was used to solve the problem due to its large radius of convergence and the relative simplicity of the flow region geometry. A relaxation factor of 0.5 was used to improve the rate of convergence. The fluid density and viscosity were  $1000 \text{ kg m}^{-3}$  and 3.5 cP, respectively. A parabolic velocity profile was imposed at the entrance of the flow region for steady flow. Under pulsatile flow, the time-dependent longitudinal component of the total normal stress ( $\sigma_{zz}$ ) was used as boundary condition at the inlet. The general form of this parameter is given by (see page 360 of Munson et al. 1994):

$$\sigma_{zz}(r, z, t) = -P(r, z, t) + 2\mu \frac{\partial V_z(r, z, t)}{\partial z}, \quad (2)$$

where  $P$  is the pressure,  $\mu$  is the fluid viscosity,  $V_z$  is the longitudinal velocity component of the fluid,  $r$  is the radial coordinate,  $z$  is the longitudinal coordinate, and  $t$  is time. Because the entrance length was long enough, the term  $\mu \partial V_z / \partial z$  is negligible and the pressure  $P$  does not vary with  $r$  at the inlet, so that  $\sigma_{zz}(z_{\text{inlet}}, t) \approx -P(z_{\text{inlet}}, t)$ . By assuming that the pressure drop due to turbulence is negligible and  $P(z_{\text{outlet}}) = 0$ , then the inlet pressure can be written as a function of the pressure gradient:  $P(z_{\text{inlet}}, t)$

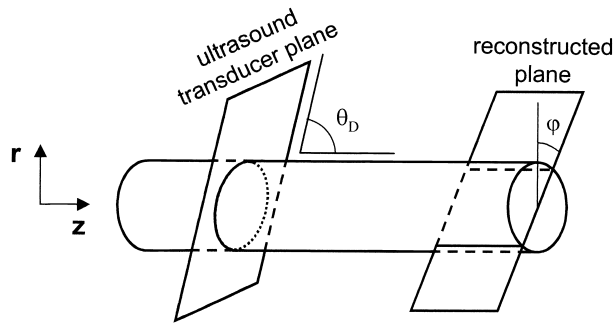


Fig. 2. Definition of the coordinates involved in the computation of eqn (3). The figure only displays a straight segment of the simulated vessel. The coordinates were used for the projection of the velocity components simulated before, within and after the stenosis.

$\approx L\Delta P(t)$ , where  $L$  is the length of the vessel and  $\Delta P$  is the pressure gradient. The parameter  $\Delta P(t)$  was estimated from the Womersley method (McDonald 1974) by using the flow rates of Fig. 1. In the simulation, the length of the vessel and the variation of the tube diameter were obtained from the *in vitro* flow model characteristics.

Based on the velocities obtained with the FEM simulations, the Doppler-shifted frequencies were calculated at each point of the mesh by using the following equation:

$$F(r, z, t) = 2F_0(V_r(r, z, t)\sin\theta_D \cos\varphi + V_z(r, z, t)\cos\theta_D)/c, \quad (3)$$

where  $F$  is the Doppler frequency shift,  $F_0$  is the ultrasound transmitted frequency,  $V_r$  and  $V_z$  are the axial and longitudinal velocity components of the fluid,  $\theta_D$  is the Doppler angle, and  $\varphi$  is the angle between the reconstructed image plane used for the FEM visualization and the vertical axis. Figure 2 describes the coordinates used in eqn (3). Only the points of the mesh whose frequency

$F$  was greater than the wall filter cut-off frequency (25 Hz) were used in the theoretical reconstruction of the stenosis geometry (theoretical binary PDA image). To simulate the persistence used with the US instrument, eqn (3) was computed at each node by taking the maximum of each Doppler shift over time. For pulsatile flow, the maxima were determined over one flow cycle. In PDA mode, the persistence of the instrument affects the displayed power intensity, whereas it is the velocities at each node that were modified by the simulated persistence function (maximum frequency shift). It should be noted that the image processing performed by the manufacturer when the persistence function is activated in PDA or color-flow velocity mode is unknown.

### Statistical analyses

All data were expressed as means  $\pm$  one standard deviation (SD). Analyses of variance (ANOVA) were used to assess differences in the means of  $E_{AR}$  as a function of the segmentation algorithm, type of fluid, type of flow and flow rate for each of the four positions along the vessel axis (SigmaStat statistical software, SPSS, San Rafael, CA, version 2.03). Nonparametric ANOVA tests (ANOVA on ranks) were used in the cases of nonGaussian statistical distributions. Pairwise multiple comparisons were performed with the Tukey test for all ANOVA. A value of  $p < 0.05$  was considered significant.

## RESULTS

### Effect of the segmentation algorithm on the percentages of area reduction

To test the effect of the segmentation algorithm on  $E_{AR}$ , the data from all measurements were pooled and compared for the four positions along the simulated vessel (one-way ANOVA). As shown in Table 1, the percentages of area reduction were overestimated by more than 4.2% before the stenosis, for all algorithms.

Table 1. Errors in the estimate of the percentage of area reduction ( $E_{AR}$ ) for four locations along the simulated artery, as a function of the segmentation algorithm selected

	Before the stenosis, mean $\pm$ SD (%)	In the stenosis, mean $\pm$ SD (%)	Recirculation zone, mean $\pm$ SD (%)	After the stenosis, mean $\pm$ SD (%)
Algorithm #1	4.2 $\pm$ 4.7	-13.0 $\pm$ 4.2	12.2 $\pm$ 12.0	6.1 $\pm$ 4.1 (*#1 vs. #3)
Algorithm #2	4.3 $\pm$ 4.8	-2.3 $\pm$ 4.0 (*#2 vs. #1 and #3)	15.0 $\pm$ 15.5	6.4 $\pm$ 4.7 (*#2 vs. #3)
Algorithm #3	6.1 $\pm$ 6.6	-5.8 $\pm$ 5.0 (*#3 vs. #1)	14.6 $\pm$ 13.7	7.9 $\pm$ 5.0

The means and standard deviations (SD) were computed over 120 measurements (all data) performed under steady and pulsatile flows, by using porcine whole blood and porcine blood cell suspension with and without US contrast agent, at flow rates of 100, 450 and 800 mL min<sup>-1</sup>. \*Statistically significant interactions ( $p < 0.05$ ) of the one-way ANOVA tests.

Table 2. Errors in the estimate of the percentage of area reduction ( $E_{AR}$ ) for four locations along the simulated artery, as a function of the type of fluid circulating in the flow model

	Before the stenosis, mean $\pm$ SD (%)	In the stenosis, mean $\pm$ SD (%)	Recirculation zone, mean $\pm$ SD (%)	After the stenosis, mean $\pm$ SD (%)
Whole blood (W)	3.3 $\pm$ 4.4 (*W vs S)	-1.7 $\pm$ 4.6	19.0 $\pm$ 14.7 (*W vs S and SC)	6.3 $\pm$ 4.9
Whole blood + contrast agent (WC)	3.3 $\pm$ 5.2 (*WC vs S)	-2.9 $\pm$ 3.3	17.1 $\pm$ 16.1 (*WC vs S and SC)	5.2 $\pm$ 5.5
Cell suspension (S)	6.6 $\pm$ 5.3	-2.0 $\pm$ 4.4	11.0 $\pm$ 15.4	7.6 $\pm$ 3.2
Cell suspension + contrast agent (SC)	4.1 $\pm$ 3.5	-2.5 $\pm$ 3.8	12.8 $\pm$ 15.1	6.5 $\pm$ 4.8

The means and standard deviations (SD) were computed over 30 measurements performed under steady and pulsatile flows of 100, 450 and 800 mL min<sup>-1</sup>. Segmentation algorithm #2 was used. \*Statistically significant interactions ( $p < 0.05$ ) of the three-way ANOVA tests.

Because the  $\%A_{R(\text{true})}$  is zero at this position, this means that artefactual narrowing of the vessel lumen was measured. No significant difference was found in the values of  $E_{AR}$  computed from the three segmentation algorithms before the stenosis ( $p = 0.28$ ). Within the stenosis, significant differences were observed ( $p < 0.001$ ). Algorithm #2 outperformed all others with a mean underestimation of the  $\%A_R$  of 2.3% (the 80% area reduction stenosis was identified as a 77.7% stenosis). An important overestimation of the  $\%A_R$  was found in the recirculation zone after the stenosis. For this position, no significant differences in the values of  $E_{AR}$  were observed when comparing the three algorithms ( $p = 0.36$ ). After the stenosis, both the first and second algorithms performed better than algorithm #3 ( $p = 0.005$ ). With the exception of measurements in the throat of the stenosis, the percentages of area reduction were always overestimated when compared to the  $\%A_{R(\text{true})}$ . In summary, algorithm #2 provided the best results in term of minimization of  $E_{AR}$ . From here on, all results are presented for the segmentation algorithm #2.

#### *Effect of the type of fluid, type of flow and flow rate on the percentages of area reduction*

Based on three-way ANOVA analyses, the differences in the mean values of  $E_{AR}$  for the different fluids were greater than what would be expected by chance for measurements performed before the stenosis ( $p = 0.006$ )

and in the recirculation zone ( $p < 0.001$ ). These results were obtained after considering the effects of differences in the type of flow and flow rate. As summarized in Table 2, the use of US contrast agent had no significant effect on  $E_{AR}$ . The statistical differences measured before the stenosis and in the recirculation zone were only related to the type of blood flowing in the phantom (whole blood or blood cell suspension). Before the stenosis,  $E_{AR}$  values were lower for whole blood than blood cell suspension, whereas it was the contrary for measurements in the recirculation zone.

Table 3 shows the differences in  $E_{AR}$  for steady and pulsatile flow measurements. The statistical method used took into consideration the effects of differences in the type of fluid and flow rate. Statistically significant differences (three-way ANOVA) were found before the stenosis ( $p < 0.001$ ) and in the recirculation zone ( $p < 0.001$ ). The errors in the percentages of area reduction were smaller for steady flow before the stenosis. In the recirculation zone, the values of  $E_{AR}$  for steady flow were approximately twice those observed for pulsatile flow. The effect of the flow rate on  $E_{AR}$  was mainly noted at 100 mL min<sup>-1</sup> (Table 4). The three-way ANOVA analyses confirmed the effect of the flow rate on  $E_{AR}$  in the stenosis ( $p < 0.001$ ), in the recirculation zone ( $p < 0.001$ ), and after the stenosis ( $p < 0.001$ ). With the exception of the measure before the stenosis, the mean values of  $E_{AR}$  monotonically increased with a decrease of

Table 3. Errors in the estimate of the percentage of area reduction ( $E_{AR}$ ) for four locations along the simulated artery, as a function of the type of flow

	Before the stenosis, mean $\pm$ SD (%)	In the stenosis, mean $\pm$ SD (%)	Recirculation zone, mean $\pm$ SD (%)	After the stenosis, mean $\pm$ SD (%)
Steady flow (S)	2.1 $\pm$ 3.0 (*S vs P)	-2.5 $\pm$ 5.2	21.1 $\pm$ 18.8 (*S vs P)	6.9 $\pm$ 4.1
Pulsatile flow (P)	6.6 $\pm$ 5.2	-2.0 $\pm$ 2.3	8.8 $\pm$ 7.1	5.8 $\pm$ 5.2

The means and standard deviations (SD) were computed over 60 measurements performed with the different fluids given in Table 2 at flow rates of 100, 450 and 800 mL min<sup>-1</sup>. Segmentation algorithm #2 was used. \*Statistically significant ( $p < 0.05$ ) interactions of the three-way ANOVA tests.

Table 4. Errors in the estimate of the percentage of area reduction ( $E_{AR}$ ) for four locations along the simulated artery, as a function of the flow rate

	Before the stenosis, mean $\pm$ SD (%)	In the stenosis, mean $\pm$ SD (%)	Recirculation zone, mean $\pm$ SD (%)	After the stenosis, mean $\pm$ SD (%)
100 mL min <sup>-1</sup>	3.9 $\pm$ 5.4	-5.9 $\pm$ 3.8 (*100 vs 450 and 800)	29.2 $\pm$ 17.3 (*100 vs 450 and 800)	9.8 $\pm$ 6.0 (*100 vs 450 and 800)
450 ml min <sup>-1</sup>	4.7 $\pm$ 3.8	-1.1 $\pm$ 3.0	10.2 $\pm$ 8.5 (*450 vs 800)	4.8 $\pm$ 2.4
800 ml min <sup>-1</sup>	4.3 $\pm$ 5.1	-0.1 $\pm$ 2.5	5.4 $\pm$ 5.5	4.6 $\pm$ 2.6

The means and standard deviations (SD) were computed over 40 measurements performed under steady and pulsatile flows by using the different fluids given in Table 2. Segmentation algorithm #2 was used. \*Statistically significant ( $p < 0.05$ ) interactions of the three-way ANOVA tests.

the flow rate. These last results considered the effect of differences in the type of flow and type of fluid.

The results reported in Tables 2 to 4 can be summarized as follows: 1. the hemodynamic condition (type of flow and flow rate) and the fluid selected (whole blood or blood cell suspension) affect the accuracy of PDA; 2. the enhancement of the echo intensity with US contrast agent has no effect on the segmentation performance; 3. the errors in the estimate of the percentages of area reduction are not uniform along the simulated atherosclerotic artery; 4. the smallest  $E_{AR}$  are usually found in the throat of the stenosis; 5. the largest errors are measured in the recirculation zone (the use of whole blood under a steady flow of 100 mL min<sup>-1</sup> emphasizes this effect); and 6. for all positions along the vessel, a low flow has a negative impact on  $E_{AR}$ . For the five experiments that would correspond to a US scan of a typical common femoral artery (whole blood, pulsatile flow of 450 mL min<sup>-1</sup>, no US contrast agent), the values of  $E_{AR}$  were 4.3  $\pm$  1.2% before the stenosis, -2.0  $\pm$  1.0% in the stenosis, 11.5  $\pm$  3.1% in the recirculation zone, and 2.8  $\pm$  1.7% after the stenosis, respectively. Figure 3 shows examples from one of these experiments of the variation of the  $\%A_R$  along the simulated vessel for pulsatile flow rates of 100, 450 and 800 mL min<sup>-1</sup>. It is clear from this figure that  $E_{AR}$  is affected by a reduction of the flow rate, and this effect is especially noticeable in the recirculation zone. Figure 4 presents the  $\%A_R$  as a function of the position along the tube for porcine whole blood circulating under a steady flow rate of 100 mL min<sup>-1</sup>. As noted before, in Table 3, the major difference between steady and pulsatile flow on the segmentation performance of PDA images is mainly noted in the recirculation zone (see Fig. 3a for comparison).

#### Comparison of measured and simulated PDA images

To understand the nature of the signal loss in the recirculation zone, the experimental PDA images of the stenosis were compared qualitatively to the simulated

images obtained under steady and pulsatile flows. The left panels of Fig. 5 show the simulated binary PDA images for steady flow; the white color indicates the presence of flow and black means the absence of echoes. In the simulations, the absence of echoes within the tube (identified by dotted lines) is due to the effect of the wall filter (Doppler frequency shifts, when projected on the transducer axis, below 25 Hz). The right panels of Fig. 5 present 2-D angle-corrected PDA images obtained by selecting the vertical image plane of the 3-D volumes ( $\varphi = 0^\circ$  in eqn (3), the top of the images corresponds to the upper surface of the flow phantom). At 100 mL min<sup>-1</sup>, the FEM simulation shows that the wall filter has an important impact on the low-velocity signal loss in the recirculation zone. The length of the stenosis appears longer than it really is. Some losses of the signal are also noted along the vessel wall. These observations are comparable to those of the corresponding PDA images. At 450 mL min<sup>-1</sup>, the FEM simulation predicted a loss of signal in the shear layer between the jet and the recirculation zone. When projected on the transducer axis, the simulated flow velocity components in the shear layer were below 0.5 cm/s (25 Hz). The shear layer was not obvious on the experimental PDA images. However, this signal loss created some blurring in the recirculation zone. The simulation performed at 800 mL min<sup>-1</sup> also predicted the signal loss in the shear layer. This time, it could not be inferred from the experimental image because it was much thinner. The 3-D reconstruction of the PDA image adequately depicted the shape of the diseased vessel at 800 mL min<sup>-1</sup>.

Figure 6 shows the comparison of the FEM simulation with a typical experiment at a pulsatile flow of 100 mL min<sup>-1</sup>. A perfect recovery of the shape of the diseased vessel was predicted by the simulation. The vertical 2-D slice of the experimental 3-D volume ( $\varphi = 0^\circ$ ) adequately matched the simulation. The signal loss previously observed in the recirculation zone under a steady flow rate of 100 mL min<sup>-1</sup> disappeared. Similar theoretical predictions and experimental results were obtained at higher flow rates (results not shown).

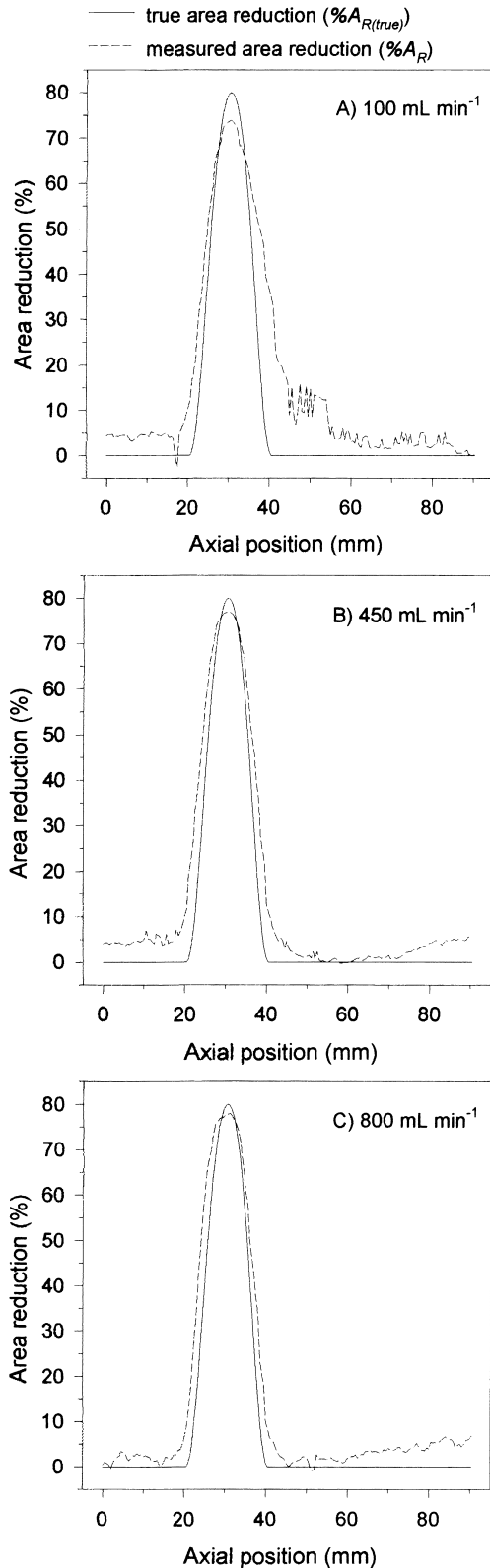


Fig. 3. Percentage of area reduction as a function of the position along the tube for typical experiments performed with porcine whole blood circulating under pulsatile flow rates of (A)  $100 \text{ mL min}^{-1}$ , (B)  $450 \text{ mL min}^{-1}$ , and (C)  $800 \text{ mL min}^{-1}$ .

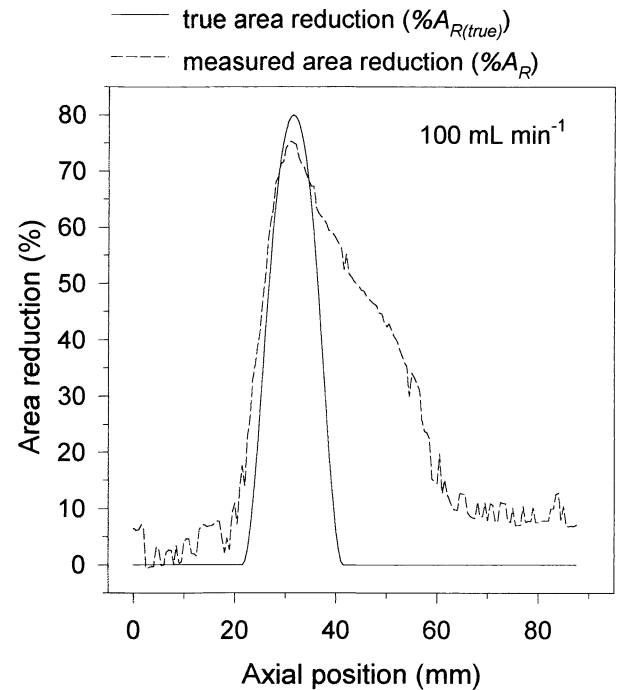


Fig. 4. Percentage of area reduction as a function of the position along the tube for a typical experiment performed with porcine whole blood circulating under a steady flow rate of  $100 \text{ mL min}^{-1}$ .

#### Observations on blood echogenicity

Longitudinal and radial variations in blood echogenicity were observed on the PDA images. As noted in Fig. 5, for whole blood flowing under a steady flow rate of  $100 \text{ mL min}^{-1}$ , the signal intensity was stronger around the central axis for all positions along the vessel. At higher flow rates (Fig. 5), the intensities of the experimental PDA images were more uniform. Some variations of the echogenicity were also noted with whole blood under pulsatile flow. As seen in Fig. 6, for a flow rate of  $100 \text{ mL min}^{-1}$ , the echo intensity varied longitudinally and radially, and it was maximum in the throat of the stenosis. Longitudinal variations of the echogenicity were more evident for experiments performed with a blood cell suspension. As seen in Fig. 7 ( $450 \text{ mL min}^{-1}$ ), the echo intensities were stronger after the stenosis than before. This phenomenon was emphasized for steady flow. Similar observations were noted at a higher flow rate of  $800 \text{ mL min}^{-1}$  (results not shown). With US contrast agents, the echogenicity was generally more uniform within the vessel.

#### DISCUSSION

Power Doppler angiography has been developed to overcome some of the limitations of color Doppler im-

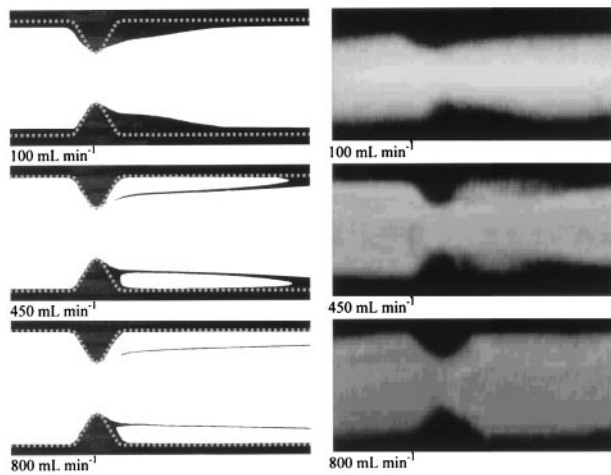


Fig. 5. Comparison of simulated (left panel) and experimental (right panel) PDA images obtained with porcine whole blood under steady flow rates of 100, 450 and 800 mL min<sup>-1</sup>. The 2-D views of both simulated and experimental PDA images were obtained from the 3-D volumes by selecting a plane parallel to the transducer axis (the top of the images corresponds to the upper surface of the flow phantom).

aging to map the blood flow field (MacSweeney *et al.* 1996; Rubin *et al.* 1994). This technique is more sensitive to blood motion than color Doppler flow, has a better signal-to-noise ratio, and is less affected by aliasing and Doppler angle. PDA was shown *in vitro* to be relatively accurate for quantifying moderate obstructions in terms of percentage of area reduction (Guo *et al.* 1998). By

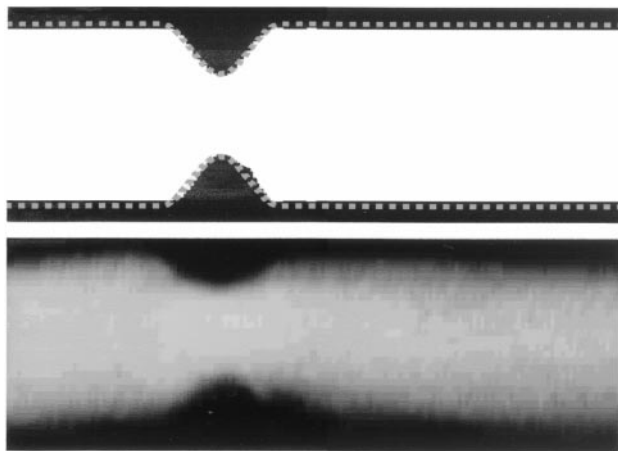
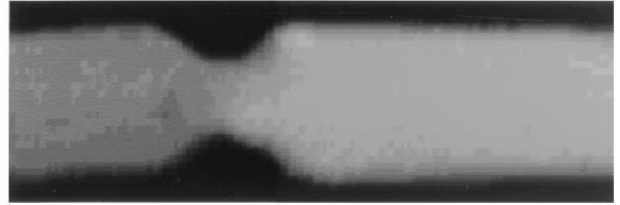


Fig. 6. Comparison of simulated (top panel) and experimental (bottom panel) PDA images for the case of porcine whole blood under a pulsatile flow rate of 100 mL min<sup>-1</sup>. The 2-D views of the PDA images were obtained from the 3-D volumes by selecting a plane parallel to the transducer axis (the top of the images corresponds to the upper surface of the flow phantom).

#### Steady flow



#### Pulsatile flow

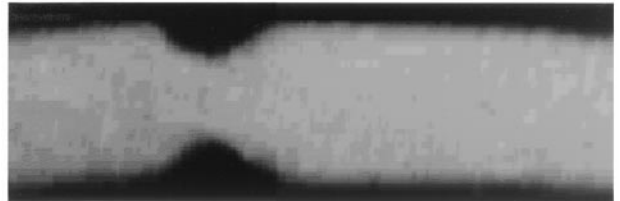


Fig. 7. 2-D views of PDA images obtained with blood cell suspension at steady and pulsatile flow of 450 mL min<sup>-1</sup>. The 2-D views of the 3-D volumes were selected parallel to the transducer axis (the top of the images correspond to the upper surface of the flow phantom).

using a blood-mimicking fluid (water-glycerol mixture with scattering particles), a 50% area reduction stenosis was quantified, on average, as a 46% stenosis. Less accurate results were obtained with a 80% stenosis. For instance, this stenosis severity was identified as a 70% lesion on average (Guo *et al.* 1998). By using porcine whole blood in a similar flow phantom, Allard *et al.* (1997) detected the 80% area reduction stenosis as a 54 to 71% lesion (mean % $A_R$  = 65%). In both studies (Allard *et al.* 1997; Guo *et al.* 1998), PDA measurements were performed with an ATL-HDI Ultramark 9 system and the segmentation of the US angiographic images was obtained with algorithm #1 (the segmentation level was fixed to 25% of the maximum image intensity,  $I_{max}$ ). The difference in accuracy between both studies can be related to the scattering properties of the fluid (blood mimic or whole blood), the flow characteristic (steady or pulsatile), and the flow rate (300 to 900 mL min<sup>-1</sup> or 120 to 1250 mL min<sup>-1</sup>).

Unpublished preliminary experiments have also been performed to test the accuracy of PDA to quantify unobstructed straight vessels of different diameters. Although the gain setting could bias the results,<sup>1</sup> we generally noted an underestimation of the true area for the largest vessels tested (diameters of 5 and 8 mm) and an overestimation for vessels smaller than 2 mm in diameter, approximately. We then hypothesized that the signal loss for the largest vessels was due to the effect of the

<sup>1</sup>A bias can exist for absolute area measurements but, in terms of percentage of area reduction, there is no bias introduced by the gain because it is a relative measure, see eqn (1).

wall filter, whereas the blurring effect for the smallest tubes could be related to the limited spatial resolution of the PDA images. To overcome the blurring effect in the throat of the stenosis, segmentation algorithm #2 was proposed. According to Table 1, this approach allowed significant reduction of  $E_{AR}$  in the stenosis when compared to previous studies for which the stenosis was underestimated by more than 9% (Allard et al. 1997; Guo et al. 1998). A third algorithm was tested to consider the histogram of the PDA image intensities. It was expected that this approach could be less affected by changes in echogenicity attributed to variations in the hemodynamic flow conditions. This algorithm did not perform better than algorithm #2. Other segmentation strategies based on the Markov field approach were recently tested on PDA images (Savéry et al. 1999). We also attempted to simply remove the background (black) from the PDA images, but this method produced large variability. It became clear to us that the optimization of more sophisticated methods is difficult because the PDA images obtained with ATL-HDI Ultramark 9 systems are limited in term of dynamic range (14 grey-level intensities logarithmically compressed) and spatial resolution. The use of the latest generation of US systems may improve the accuracy of PDA. Further studies would, however, be necessary to determine the extent of this potential improvement, as well as that of other segmentation strategies.

#### *Observations on blood echogenicity*

It is known that porcine whole blood forms red blood cell (RBC) aggregates under certain flowing conditions, and that red cells suspended in a saline solution do not form aggregates, whatever the value of the flow shear rate. It is also well recognized that RBC aggregation increases the echogenicity of blood (Sigel et al. 1982), and that this phenomenon is promoted at low shear rates (Schmid-Schönbein et al. 1968). As shown in Fig. 5, for a flow rate of  $100 \text{ mL min}^{-1}$ , the level of RBC aggregation can affect the radial distribution of blood echogenicity; a similar observation was recently reported by Allard and Cloutier (1999). RBC aggregation can also modify the echogenicity before, within and after the stenosis (see Fig. 6). In addition to RBC aggregation, other factors can affect the echogenicity of blood. For example, by using A-mode pulse-echo and Doppler US methods, turbulence was shown to significantly increase the US backscattered power (Cloutier et al. 1996; Shung et al. 1984). This phenomenon has been observed for red cells suspended in saline, but has never been demonstrated for whole blood experiments. According to Fig. 7, an increase in blood echogenicity for experiments performed with a blood cell suspension could be observed on PDA after the stenosis. These echoicity variations are likely due to the presence of blood flow turbulence. It is interesting to note that the use of whole blood under the

same hemodynamic flow conditions did not produce the same effect on the PDA images (see Figs. 5 and 6). The mechanisms explaining these differences still remain to be explored.

#### *Effect of the type of fluid, type of flow and flow rate on the percentages of area reduction*

According to Table 2, the use of whole blood or blood cell suspension influenced the accuracy of the PDA image segmentation before the stenosis and in the recirculation zone. The presence of RBC aggregation in some experiments (especially those performed at  $100 \text{ mL min}^{-1}$ ), and the effect of turbulence on the echogenicity of blood cell suspension may explain the differences in  $E_{AR}$  at these locations. Axial and radial echogenicity variations affect the value of  $I_{\max}$  that was used in the segmentation algorithm #2. These echogenicity variations can also modify the histogram distribution of the PDA image intensities. Figure 8 shows histograms corresponding to the PDA image of Fig. 7 for the case of steady flow (top panel). This example, which corresponds to an experiment without RBC aggregation, can explain the differences found in Table 2 before the stenosis. It is clear from Fig. 8 that  $I_{\max}$  and the histogram distribution changed along the vessel. If we assume a constant segmentation level at 25% of  $I_{\max}$  for this example, the threshold is 40 for frame #10 and 45 for frame #110. Because of the discrete nature of the histograms, the segmentation threshold is, in fact, the same for both 2-D frames. The higher  $E_{AR}$  before the stenosis for blood cell suspension is explained by the fact that the proportion of echoes removed was higher before than after the stenosis (for the example of Fig. 8, 6480 and 5862 pixels were removed before and after the stenosis, respectively; the total number of pixels was 13,875).

One important hemodynamic consequence of the presence of RBC aggregation is the increase in blood viscosity (Chien 1967). The flow characteristics and the effects of RBC aggregate formation may specifically explain the differences noted in Table 2 for the recirculation zone. For example, the signal loss in the recirculation zone was more important for whole blood than blood cell suspension. The presence of RBC aggregation and a higher viscosity may result in lower flow velocity components and the removal of more echoes by the wall filter. The validation of this hypothesis would require the use of a non-Newtonian fluid in the finite-element modeling of the blood flow velocities.

According to Table 3, the type of fluid significantly influenced the segmentation results before the stenosis and in the recirculation zone. As demonstrated by the finite-element modeling of Fig. 5, the wall filter is the cause of the signal loss under steady flow in the recircu-

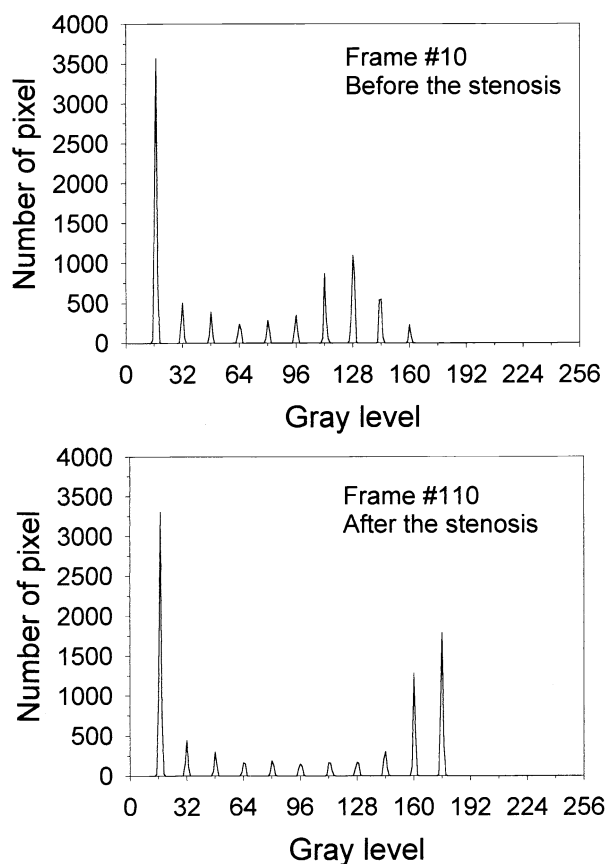


Fig. 8. Histograms of the pixel intensities, in grey level, of the PDA image of Fig. 7 for the case of steady flow. The frame number corresponds to the position of the cross-section in the 3-D volume (total number of frames = 180). The grey level of 16 corresponds to the background noise of the PDA image. To display the text, the instrument uses the maximum intensity level (white, *i.e.*, 256). A total of 14 discrete grey levels were used to map the backscattered power. For each level, the histogram is not a Dirac function because of the uncertainties (noise) introduced by the analog link between the ATL instrument and the 3-D acquisition system (digital-to-analog conversion of the ATL instrument to generate the analog video signal, and analog-to-digital conversion of the 3-D acquisition system to reproduce the digital video image).

lation zone. The higher  $E_{AR}$  before the stenosis for pulsatile flow cannot be explained by axial and radial variations of blood echogenicity. For example, we noted that pulsatile flow had the tendency to limit any echogenicity changes, probably because pulsatility has a negative effect on RBC aggregation (Riha and Stoltz 1996). It is postulated that vessel pulsation due to the presence of a tight stenosis downstream might explain the higher  $E_{AR}$  before the stenosis for pulsatile flow. The agar flow phantom used in this study is known to be compliant (de Korte *et al.* 1997). When blood accelerated during systole, the vessel diameter could increase momentarily,

whereas it probably decreased below the expected true diameter for the rest of the flow cycle. Because the duration of diastole was higher than systole, the  $\%A_R$  was overestimated by 6.6% on average.

As predicted by the finite-element modeling of Fig. 5, a low flow rate should increase  $E_{AR}$  for all positions along the vessel, except in the throat of the stenosis. As seen in Table 4, contradictory results were obtained experimentally in the stenosis. For example, the percentage of area reduction at this position was underestimated by 5.9% on average at a flow rate of  $100 \text{ mL min}^{-1}$ . For all other flow rates, the errors were below 1.1%. Because the true area is not known in practice, we computed the percentage of area reduction based on a reference area,  $A_{\text{ref}}$ , defined as the 10 largest area values of the PDA images along the vessel. In clinical practice, this would be the optimal method to use. However, because  $A_{\text{ref}}$  was biased because the wall filter removes echoes along the vessel wall at  $100 \text{ mL min}^{-1}$ , the computation of eqn (1) artificially underestimated the percentage of area reduction in the stenosis. The statistically largest  $E_{AR}$  found in Table 4, for measurements in the recirculation zone and after the stenosis, are due to the wall filter.

#### Other considerations

The use of a high persistence during the recording of the PDA images seemed important to adequately describe the shape of the stenosis along its longitudinal axis. The selection of the maximum persistence of 7 provided the best signal-to-noise ratio of the images. Under pulsatile flow, it also permitted reduction of the signal loss in the recirculation zone due to the effect of the wall filter. During the acceleration and deceleration of the flow, the length of the recirculation zone and the velocities within it vary considerably. The simulations of the binary PDA images with Fidap showed that the use of the maximum velocity at each node instead of the time-averaged velocities, for example, best mimicked the high persistence mode of the US instrument.

## CONCLUSIONS

It was shown that longitudinal and radial changes in blood echogenicity, the attenuation of echoes by the wall filter, the limited spatial resolution and dynamic range of the US instrument, and possible vessel pulsation proximal to the stenosis, can all affect the accuracy of PDA. In the present study, the purpose of using a blood cell suspension (no RBC aggregation) was to compare the results with whole blood, for which the presence of RBC aggregates at low flow shear rates is well documented. It may be relevant to know, however, that some conditions may inhibit RBC aggregation and lead to PDA images similar to those presented in this study for experiments

performed with blood cell suspension. Examples include patients with a high concentration of plasma albumin, a low concentration of plasma fibrinogen or immunoglobulins, or the use of PEG-coated RBC blood substitutes (Armstrong et al. 1997).

In previous studies on PDA (Allard et al. 1997; Guo et al. 1998; Guo and Fenster 1996), steady flow was used in the flow models. In the present study, the use of steady flow and the FEM simulations of PDA images with Fidap allowed a clear evaluation of the effect of the wall filter on the signal loss in the recirculation zone. The wall filter also explained the overestimation of the length of the stenosis in some experiments. For conditions that would correspond to a US scan of a typical common femoral artery (whole blood circulating at a pulsatile flow of  $450 \text{ mL min}^{-1}$ ), the errors in the percentages of area reduction were  $4.3 \pm 1.2\%$  before the stenosis,  $-2.0 \pm 1.0\%$  in the stenosis,  $11.5 \pm 3.1\%$  in the recirculation zone, and  $2.8 \pm 1.7\%$  after the stenosis, respectively. The use of the latest generation of US systems should improve the accuracy because of the enhanced image resolution and dynamic range. One difficulty encountered with the segmentation algorithms was the non-uniform echogenicity along the vessel. It would be relevant for angiographic applications to damp out these variations by using a more severe logarithmic compression of the images.

The results of this study showed that 3-D angiographic images could be obtained with PDA. The better understanding of the parameters that influence the stenosis analysis should allow improvement of the diagnostic accuracy of this technique. The role of US contrast agents in this approach remains to be demonstrated. Potential clinical applications of an angiographic mapping by using PDA are numerous because this technology is far less invasive than intra-arterial angiography and less expensive than magnetic resonance angiography. Because PDA is used extensively to image low-flow in small vessels (Bearcroft et al. 1996; Bude et al. 1994), it may improve the diagnosis of lower limb distal segments below the knee and runoff arteries. PDA may also allow detection of stenoses in low-flow segments distal to occluded or highly stenotic vessels. Its high accuracy in detecting moderate stenoses is attractive and, more interestingly, this diagnostic method is not affected by the presence of multiple stenoses (Guo et al. 1998).

*Acknowledgements*—This work was supported by the Medical Research Council of Canada (MA-14985) and the Heart and Stroke Foundation of Québec. The authors thank Dr. Champlain Landry, Mr. David Savéry and Ms. Isabelle Fontaine (IRCM, Montréal, Québec, Canada) for helpful discussions, Dr. Helen Routh (Advanced Technology Laboratories) for loaning the ATL Ultramark 9 HDI US system, Dr. Aaron Fenster (John Robarts Institute, London, Ontario, Canada) for technical support, Life Imaging System (London, Ontario, Canada) for providing the 3-D imaging

software, and Dr. Martin L. Rosenberg, Dupont-Merck (N. Billerica, MA) for providing the DMP-115 US contrast agent.

## REFERENCES

- Allard L, Cloutier G. Power Doppler ultrasound scan imaging of the level of red blood cell aggregation: An *in vitro* study. *J Vasc Surg* 1999;30:157–168.
- Allard L, Cloutier G, Fenster A, Durand LG. 3-D power Doppler ultrasound imaging of an *in vitro* arterial stenosis. In: S Lees, LA Ferrari, eds. *Acoustical imaging*. New York: Plenum Press, 1997: 267–272.
- Allard L, Cloutier G, Guo Z, Durand LG. Review of the assessment of single level and multilevel arterial occlusive disease in lower limbs by duplex ultrasound. *Ultrasound Med Biol* 1999;25:495–502.
- Aly S, Jenkins MP, Zaidi FH, Coleridge Smith PD, Bishop CC. Duplex scanning and effect of multisegmental arterial disease on its accuracy in lower limb arteries. *Eur J Vasc Endovasc Surg* 1998a;16:345–349.
- Aly S, Sommerville K, Adishesiah M, Raphael M, Coleridge Smith PD, Bishop CC. Comparison of duplex imaging and arteriography in the evaluation of lower limb arteries. *Br J Surg* 1998b;85:1099–1102.
- Armstrong JK, Meiselman HJ, Fisher TC. Covalent binding of poly-(ethylene glycol) (PEG) to the surface of red blood cells inhibits aggregation and reduces low shear blood viscosity. *Am J Hematol* 1997;56:26–28.
- Bearcroft PW, Berman LH, Robinson AHN, Butler GJ. Vascularity of the neonatal femoral head: *In vivo* demonstration with power Doppler US. *Radiology* 1996;200:209–211.
- Bude RO, Rubin JM, Adler RS. Power versus conventional color Doppler sonography: Comparison in the depiction of normal intrarenal vasculature. *Radiology* 1994;192:777–780.
- Chien S. Blood viscosity: Influence of erythrocyte aggregation. *Science* 1967;157:829–831.
- Cloutier G, Allard L, Durand LG. Characterization of blood flow turbulence with pulsed-wave and power Doppler ultrasound imaging. *J Biomech Eng* 1996;118:318–325.
- de Korte CL, Céspedes EI, Van der Steen AFW, Norder B, te Nijenhuis K. Elastic and acoustic properties of vessel mimicking material for elasticity imaging. *Ultrasonic Imaging* 1997;19:112–126.
- Dedichen H, Kordt KF. Blood flow in normal human ileo-femoral arteries studied with electromagnetic technique. *Acta Chirurg Scand* 1974;140:371–376.
- Evans DH, McDicken WN, Skidmore R, Woodcock JP. *Doppler ultrasound, physics, instrumentation, and clinical applications*. Chichester, New York, Brisbane, Toronto, Singapore: John Wiley & Sons, 1989.
- Guo Z, Fenster A. Three-dimensional power Doppler imaging: A phantom study to quantify vessel stenosis. *Ultrasound Med Biol* 1996;22:1059–1069.
- Guo Z, Durand LG, Allard L, Cloutier G, Fenster A. *In vitro* evaluation of multiple arterial stenoses using three-dimensional power Doppler angiography. *J Vasc Surg* 1998;27:681–688.
- Hlavová A, Linhart J, Prerovský I, Ganz V, Froněk A. Leg blood flow at rest, during and after exercise in normal subjects and in patients with femoral artery occlusion. *Clin Sci* 1965;29:555–564.
- Koelmay MJW, Legemate DA, van Gurp J, Ponson AE, Reekers JA, Jacobs MJHM. Colour duplex scanning and pulse-generated run-off for assessment of popliteal and crural arteries before peripheral bypass surgery. *Br J Surg* 1997;84:1115–1119.
- Larch E, Minar E, Ahmadi R, Schnürer G, Schneider B, Stümpflen A, Ehringer H. Value of color duplex sonography for evaluation of tibioperoneal arteries in patients with femoropopliteal obstruction: A prospective comparison with anterograde intraarterial digital subtraction angiography. *J Vasc Surg* 1997;25:629–636.
- London NJM, Nydahl S, Hartshorne T, Fishwick G. Use of colour duplex imaging to diagnose and guide angioplasty of lower limb arterial lesions. *Br J Surg* 1999;86:911–915.
- MacSweeney JE, Cosgrove DO, Arenson J. Colour Doppler energy (power) mode ultrasound. *Clin Radiol* 1996;51:387–390.
- McDonald DA. *Blood flow in arteries*. London: Edward Arnold, 1974.
- Munson BR, Young DF, Okiishi TH. Differential analysis of fluid flow. In: Munson BR, Young DF, Okiishi TH, eds. *Fundamentals of fluid*

- mechanics. New York, Chichester, Brisbane, Toronto, Singapore: John Wiley & Sons, 1994:309–393.
- Rickey DW, Picot PA, Christopher DA, Fenster A. A wall-less vessel phantom for Doppler ultrasound studies. *Ultrasound Med Biol* 1995;21:1163–1176.
- Riha P, Stoltz JF. Flow oscillations as a natural factor of reduction of the effect of RBC aggregation on blood flow. *Clin Hemorheol* 1996;16:43–48.
- Rubin JM, Bude RO, Carson PL, Bree RL, Adler RS. Power Doppler US: A potentially useful alternative to mean frequency-based color Doppler US. *Radiology* 1994;190:853–856.
- Savéry D, Tranulis C, Qin Z, Goussard Y, Cloutier G, Durand LG. Anatomic evaluation of arterial stenoses by power Doppler imaging using a Markov field segmentation. Proceedings of the 45th Annual Meeting of the Canadian Organization of Medical Physicists, 1999: 212–214.
- Schmid-Schönbein H, Gaetgens P, Hirsch H. On the shear rate dependence of red cell aggregation in vitro. *J Clin Invest* 1968;47: 1447–1454.
- Sensier Y, Hartshorne T, Thrush A, Handford H, Nydahi S, London NJM. The effect of adjacent segment disease on the accuracy of colour duplex scanning for the diagnosis of lower limb arterial disease. *Eur J Vasc Endovasc Surg* 1996;12:238–242.
- Shung KK, Yuan YW, Fei DY, Tarbell JM. Effect of flow disturbance on ultrasonic backscatter from blood. *J Acoust Soc Am* 1984;75: 1265–1272.
- Sigel B, Machi J, Beitler JC, Justin JR, Coelho JCU. Variable ultrasound echogenicity in flowing blood. *Science* 1982;218: 1321–1323.
- Vänttinen E. Electromagnetic measurement of the arterial blood flow in the femoropopliteal region. *Acta Chirurg Scand* 1975;141:353–359.